Aluminum Alkoxy-Catalyzed Biomass Conversion of Glucose to 5-Hydroxymethylfurfural: Mechanistic Study of the Cooperative Bifunctional Catalysis

Qing Wang,[a] Mingxing Fu,[a] Xiaojun Li,[a] Runfeng Huang,[a] Rainer E. Glaser,[b,c] and Lili Zhao ⓘ*[a]

Density functional theory calculations were performed to understand the detailed reaction mechanism of aluminum alkoxy-catalyzed conversion of glucose to 5-hydroxymethylfurfural (HMF) using $Al(OMe)_3$ as catalyst. Potential energy surfaces were studied for aggregates formed between the organic compounds and $Al(OMe)_3$ and effects of the medium were considered via continuum solvent models. The reaction takes place via two stages: isomerization from glucose to fructose (stage I) and transformation of fructose to HMF (stage II). Stage II includes three successive dehydrations, which begins with a 1,2-elimination to form an enolate (i.e., B), continues with the formation of the acrolein moiety (i.e., D), and ends with the formation of the furan ring (i.e., HMF). All of these steps are facilitated by aluminum alkoxy catalysis. The highest barriers for stage I and stage II are 23.9 and 31.2 kcal/mol, respectively, and the overall catalytic reaction is highly exothermic. The energetic and geometric results indicate that the catalyzed reaction path has feasible kinetics and thermodynamics and is consistent with the experimental process under high temperature (i.e., 120 °C). Remarkably, the released water molecules in stage II act as the product, reactant, proton shuttle, as well as stabilizer in the conversion of fructose to HMF. The metal–ligand functionality of the $Al(OMe)_3$ catalyst, which combines cooperative Lewis acid and Lewis base properties and thereby enables proton shuttling, plays a crucial role in the overall catalysis and is responsible for the high reactivity. © 2019 Wiley Periodicals, Inc.

DOI: 10.1002/jcc.25812

Introduction

The chemistry of conversion of nonfood plant biomass to fuels and chemicals has been significantly developed in the past decades.[1–13] The majority of sugars in plant biomass are stored in the form of hemicellulose and cellulose.[14] It is exciting that cellulose can be hydrolyzed into water-soluble reducing sugars with high conversion rate under the catalytic effect of mineral or organic acid,[15,16] or even without any additional catalyst in ionic liquids (ILs)–H_2O mixtures.[17] The reducing biomass sugars can be further transformed into the important biomass platform chemical 5-hydroxymethylfurfural (HMF).[18]

HMF is a multipurpose intermediate for the synthesis of high value-added chemicals and fuels,[19] and in fact, HMF production has become an important component of biomass conversion.[20–28] Since glucose is the most abundant monosaccharide, the catalyst-mediated direct conversion of glucose to HMF is particularly promising. Early attempts focused on lanthanide halide catalysts (i.e., $LnCl_3$, Ln = $La^{3+} - Lu^{3+}$), which can promote the conversion of glucose to HMF with very low yield (~10%).[29–31] Later studies found that the chromium halides ($CrCl_n$, n = 2, 3) could be the effective catalysts for the conversion of glucose into HMF. For example, Zhao et al.[32] reported that the $CrCl_2$-catalyzed reaction in the IL 1-alkyl-3-methylimidazolium chloride gives a high HMF yield of 70%. The HMF yield could be further increased to 81% by adding N-heterocyclic carbene ligand to the reaction system.[33] In 2012, Hensen and coworkers[34] reported that the conversion of glucose to HMF can be promoted by the transient Cr^{2+} dimer with rationally HMF yields (ca. 60%). In 2013, Chen group developed $CrCl_2$/imidazolium chloride systems which higher turnover rates with reasonably high HMF yields of >65%.[35] In addition, they reported that Chromium(0) nanoparticles in the $CrCl_2$/IL system were effective catalyst for the conversion of glucose to HMF.[36] Under the catalytic effect of $CrCl_3$ in DBU-based ILs (DBU = 1,8-diazabicyclo[5.4.0]undec-7-ene) and in benzenesulfonate ILs, the conversion of glucose to HMF can be significantly improved to very high HMF yields.[37,38] It should be emphasized that the ILs play key role in the chromium halide-mediated conversion reactions.[39,40] The use of $CrCl_n$ catalyst in

[a] Q. Wang, M. Fu, X. Li, R. Huang, L. Zhao
Institute of Advanced Synthesis, School of Chemistry and Molecular Engineering, Jiangsu National Synergetic Innovation Center for Advanced Materials, Nanjing Tech University, Nanjing 211816, China
E-mail: ias_llzhao@njtech.edu.cn

[b] R. E. Glaser
Department of Chemistry, University of Missouri, Columbia, Missouri 65211

[c] R. E. Glaser
Department of Chemistry, Missouri University of Science and Technology, Rolla, Missouri

Wiley Online Library

J. Comput. Chem. **2019**, *40*, 1599–1608   **1599**

BrØnsted acid solvents, such as H_2SO_4[15] or the acidic IL [EMIM][HSO_4][16] produces only 8–9% HMF yields.

Alternative to chromium halides, many efforts have also been made to develop inexpensive and less harmful catalysts for the conversion of glucose to HMF.[41] In 2009, Hu and coworkers[42] reported that the common Lewis acid $SnCl_4$ can be used as the catalyst in this conversion with 62% HMF yield. In 2010, Chidambaram and Bell found that the $H_3PMo_{12}O_{40}$/[EMIM]Cl system with acetonitrile as the cosolvent can obtain high-to-quantitative yield.[43] Later, it was found that nanophase materials, such as nano-POMs(polyoxometalates)/nano-ZrO_2/nano-γ-Al_2O_3, can be used as an effective catalyst for the conversion of glucose to HMF with yields of >60%.[44] Matsumiya et al.[45] reported in 2015 that the combination of choline dihydrogencitrate and glycolic acid can provide a yield of ~60%. Recently, Chu et al.[46] found that WO_3/RGO (reduced graphene oxide) could also catalyze the conversion of glucose to HMF.

Regardless of the impressive developments of metal halide and complex metal oxide catalysts to transform glucose into HMF, it remains a challenge to identify new catalysts for this purpose with high efficiencies that are easily accessible and less harmful to the environment. Recently, Chen and coworkers[47] made much progress in this direction with their discovery that aluminum alkyl (e.g., $AlMe_3$, $AlEt_3$) and alkoxy compounds (e.g., $Al(O^iPr)_3$, $Al(O^tBu)_3$) are also very effective catalysts for glucose-to-HMF conversion. In a more recent study, Ladipo found that the L^RAlMe_2 (L^R = (aminomethyl)phenolate) complexes are effective catalysts for the transformation of glucose to HMF in the ILs.[48] Remarkably, the aluminum alkoxy compounds have become commodity chemicals and they are much cheaper than the benchmark catalyst $CrCl_2$ (by a factor of 180 for $Al(O^iPr)_3$) and they exhibit high reactivity toward glucose-to-HMF conversion with comparable or even higher HMF yield (ca. 62%).

Intrigued by the novelty of the aluminum alkoxy catalysts, we studied the detailed reaction mechanisms of the catalytic conversion of glucose to HMF by using $Al(OMe)_3$ as a representative catalyst model. On the basis of the stabilities and the structures of the intermediates and transition states, we can consistently rationalize the origins of the high reactivity of the aluminum alkoxy catalysts. The insights gained by our mechanistic analysis suggests that the development of more efficient catalysts should focus on tuning structural features that improve the last dehydration step leading to furan formation, which can provide further synthetic strategy for experiments.

Computational Details

All calculations involved in this study were carried out by using the Gaussian 09 program.[49] Previous mechanistic study on the chromium, as well as boric acid-catalyzed dehydration of glucose to HMF in ILs indicated that the B3LYP[50,51] Density functional theory (DFT) functional calculations are reasonable for such reactions. The B3LYP functional was thus used to carry out all DFT calculations in this study. We use $Al(OMe)_3$ as the computational model of the catalysts (i.e., $Al(O^iPr)_3$). Briefly, all structures involved were optimized and characterized as minima or transition states

at the B3LYP/6-31G** level. The harmonic frequencies were computed at the same level for the zero-point energy corrections, thermal and entropic corrections at 298.15 K and 1 atm. Intrinsic reaction coordinate calculations were performed to examine the correct connections between the transition states and the corresponding minima if necessary. The relative energies were then improved by M06-2X[52]/6–311++G(2d,p)//B3LYP/6-31G(d,p) single-point calculations with solvent effects accounted by means of IEFPCM,[53–56] using the experimentally used ILs as solvent. The solute cavities were constructed using the default set of UFF atomic radii.[57] The solvent ILs was parameterized in analogy to dibromomethane (ε = 7.26). The effective solvent radius R_{solv} = 292.3 pm was derived using the Stearn–Eyring equation,[58] and the molecular density (5,000 pm^{-3}) and the molecular volume (V_{mol} = 120.25 cm^3 mol^{-1}) were obtained from the macroscopic properties of ILs (density = 1.186 g cm^{-3}, molecular mass = 142.62 g mol^{-1}). The Gibbs free energies in the solvent at the M06-2X/6–311++G(2d,p) level are used in the following discussion, unless otherwise specified, and the enthalpies are given for references in the related schemes and figures.

Results and Discussion

The goal of this study includes unveiling the detailed mechanism of the $Al(OMe)_3$-catalyzed conversation of glucose to HMF and rationalizing the origin of the reactivity of the aluminum alkoxy catalysts. In particular, we herein show that the reaction takes place via two stages (Scheme 1): the isomerization of glucose 1 to fructose 2 (stage I) and the dehydration of fructose 2 to HMF 3 (stage II). Stage II includes a series of three successive dehydrations steps, which begins with a 1,2-elimination step to form an enolate B intermediate, which is the anion form of (2R,E)-2-(hydroxymethyl)-5-(hydroxymethylene)-tetrahydrofuran-3,4-diol. The reaction continues with the formation of the acrolein moiety D, which has the resonance structure with C, and ends with the formation of the furan ring HMF 3.

Stage I: Catalytic isomerization of glucose 1 to fructose 2

The $Al(OMe)_3$-catalyzed conversion of 1 to 2 can be characterized by three steps: (1) ring-opening of the cyclic pyranose 1 to its open-chain isomer; (2) isomerization from the open-chain form of glucose to the open-chain form of fructose; and (3) ring closure generating fructose 2. Note that the direct conversion of 1 to 2 without catalyst is excluded because of the very high barriers (>48 kcal/mol; see Supporting Information Scheme S1).

Step 1: Ring-opening of glucose 1 to its open-chain isomer. As shown in Scheme 2, the initial step is the formations of the Lewis acid–base adduct IM1, which is 13.6 kcal/mol more stable than the separated $Al(OMe)_3$ and 1. After crossing a low barrier of 10.7 kcal/mol (TS1), the H1 atom of OH group in IM1 can be easily transferred to one —OMe ligand of $Al(OMe)_3$ leading to the more stable intermediate IM2 with exothermic by 5.2 kcal/mol. The activated H1-atom can further be transferred to O3-atom in the six-membered ring via a barrier of 13.8 kcal/mol (TS2) leading to IM3, which is the open-chain isomer of glucose 1.
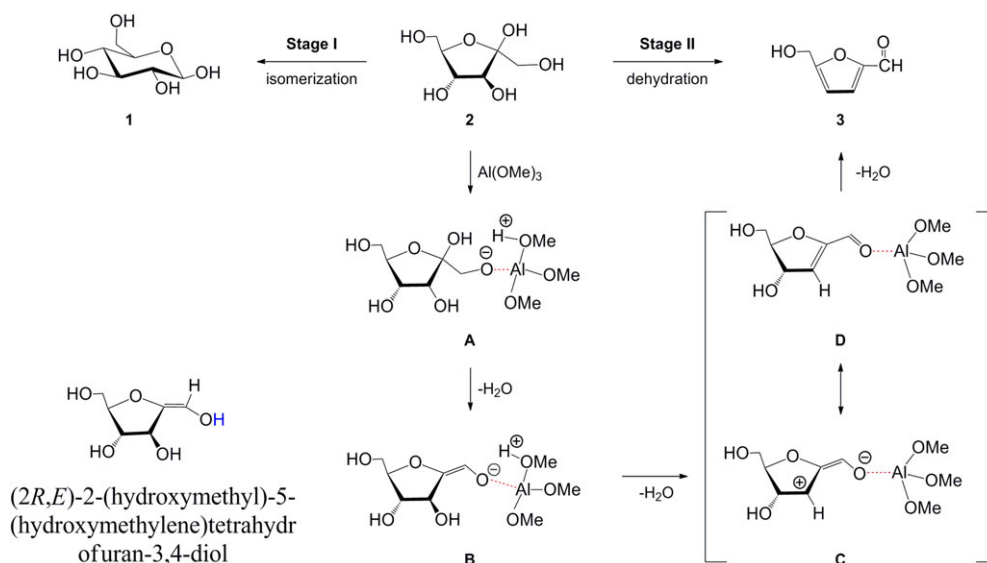
Scheme 1. Proposed mechanisms for the Al(OMe)₃-catalyzed conversation of glucose 1 to HMF 3. [Color figure can be viewed at wileyonlinelibrary.com]

(2R,E)-2-(hydroxymethyl)-5-(hydroxymethylene)tetrahydrofuran-3,4-diol

We also considered the concerted ring opening step via transition state TS1′ without the assistance of the —OMe ligand of the catalyst. However, the high barrier, which is 25.4 and 27.5 kcal/mol higher than TS1 and TS2, respectively, precluded the concerted reaction channel. It is noteworthy that the metal–ligand (i.e., Al—OMe) bifunctional effect plays a critical role in stabilizing the transition states and the intermediates, as indicated by optimized transition states in Figure 1.

In order to generate the open-chain conformation of fructose, the catalyst Al(OMe)₃ in IM3 needs slight adjustment in its position to approach to the carbonyl and the neighboring OH group leading to IM4 with a barrier of 8.2 kcal/mol (TS3). Although IM4 is 1.1 kcal/mol less stable than IM3, the subsequent steps (see Scheme 3) can provide thermodynamic driving force to move the reaction forward.

Step 2: Isomerization from the open-chain form of glucose to the open-chain isomer of fructose. Two reaction pathways for the isomerization process from the open-chain form of glucose to the open-chain form of fructose mediated by the Al(OMe)₃ catalyst were explored. Scheme 3 shows the calculated free energy profiles, and the optimized geometries of some key transition states are given in Figure 2.

The Al-atom of Al(OMe)₃ catalyst first binds to the —OH group neighboring the carbonyl group via a barrier of 9.7 kcal/mol (TS4) leading to the more stable intermediate IM5 (the black path). As shown in Scheme 3, the metal–ligand bifunctional effect plays significant role in the following hydrogen transfer process from IM5 to IM7. The hydrogen shift takes place via a stepwise mechanism: the H2-atom of —OH in IM5 is transferred to the O5-atom of —OMe by crossing the TS5
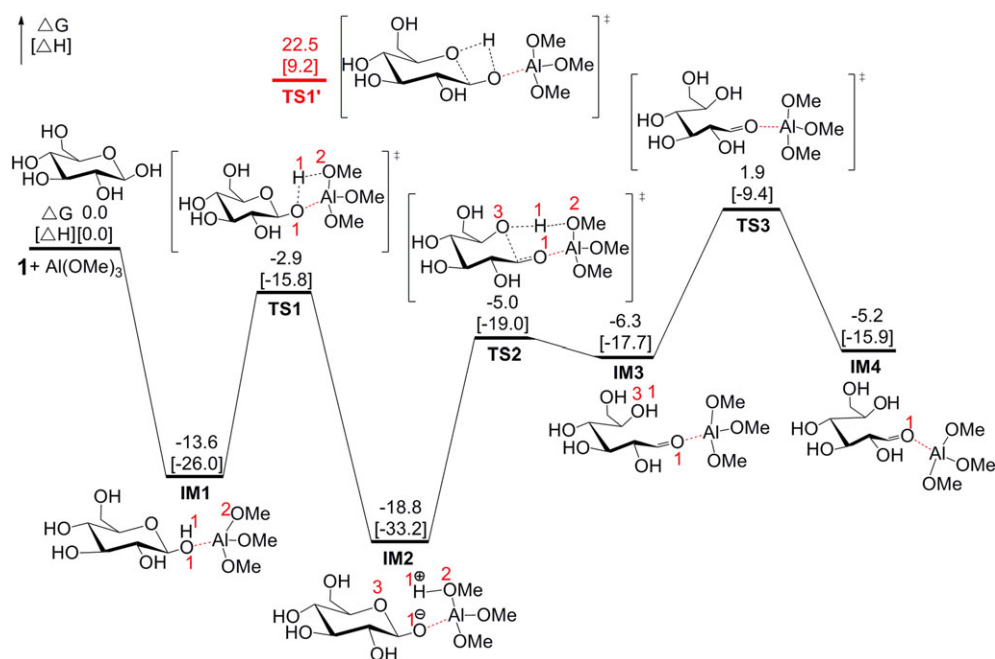
Scheme 2. Free energy profiles for the ring opening step (step 1) in stage I. Values in kcal/mol are free energies and enthalpies (in the brackets), respectively. [Color figure can be viewed at wileyonlinelibrary.com]
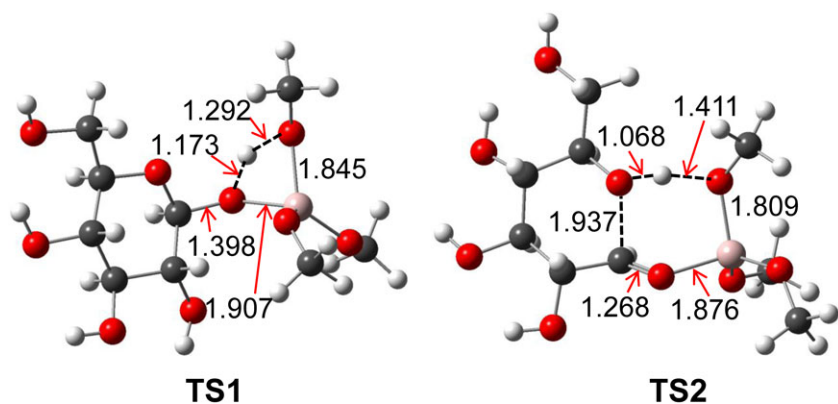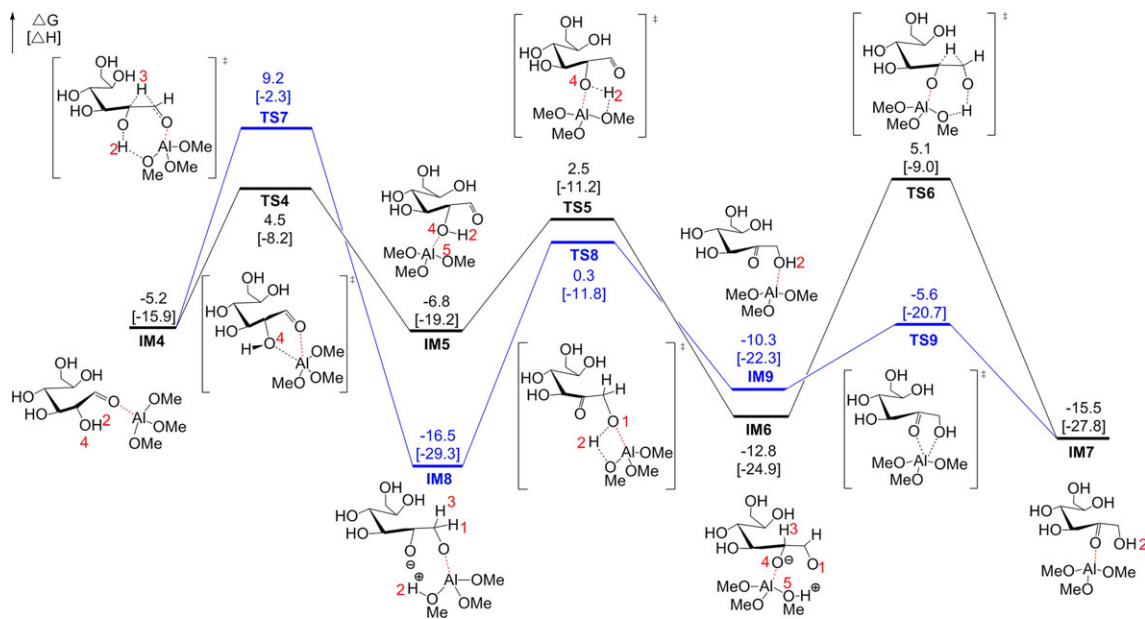
Figure 1. Optimized geometries of TS1 and TS2, along with the key bond distances in Å. Trivial hydrogen atoms are omitted for clarity (color code, C: black, H: white, O: red, Al: pink). Other structures are given in Supporting Information Figure S1. [Color figure can be viewed at wileyonlinelibrary.com]

transition state to give the more stable IM6, followed by a concerted H-shift transition state TS6 to generate the open-chain form of fructose as indicated by IM7. The barriers for the two H-transfer steps are 9.3 and 17.9 kcal/mol, respectively, which are in the range for experimental realization under mild conditions. The optimized geometries of the transition states TS5 and TS6 in Figure 2 illustrate the O—H/C—H bonds activation and following H-shifts process. IM6 and IM7 are 6.0 and 8.7 kcal/mol, respectively, more stable than IM5, implying a thermodynamic reaction channel.

An alternative mechanism was proposed on the basis of different hydrogen shift sequences. As shown the blue path in Scheme 3, the H2- and H3-atom can be simultaneously transferred to one –OMe ligand of Al(OMe)$_3$ catalyst and the carbonyl carbon atom (i.e., C^{CO}), respectively, via a concerted transition state TS7 to generate IM8. The hydrogen transfer process is illustrated by the C—H—C (1.347 and 1.391 Å) and O—H—O (1.097 and 1.336 Å) distances in TS7 (Fig. 2). By comparison, the reaction channel from IM4 to IM8 is kinetically 4.7 kcal/mol less favorable but thermodynamically 9.7 kcal/mol

more favorable than the path of IM4 → IM5. The H2—OMe moiety in IM8 then adjusts its position to release the activated H2-atom to the O1-atom by crossing a barrier of 16.8 kcal/mol (TS8) giving IM9. Although IM9 is 6.2 kcal/mol higher than IM8, the following step via a low barrier of 4.7 kcal/mol (TS9) leading to IM7 is exergonic by 5.2 kcal/mol, which can afford thermodynamic driving force. Comparisons in Scheme 3 indicated that both the scenarios for this step are reasonable for experimental realization under mild reaction conditions, but the black reaction channel is slightly kinetically favorable.

Step 3: Ring closure generating cyclic fructose 2. As indicated by Scheme 4, the —OMe ligand of Al(OMe)$_3$ also plays an important role in the ring-closure step. After overcoming a barrier of 4.2 kcal/mol (TS10), the five-membered-ring intermediate IM10 can be formed with the H4-atom of the —OH group simultaneously transferred to the —OMe ligand of Al(OMe)$_3$. The H4-OMe moiety then regulates its position to transfer the H4-atom via TS11 ($\Delta G^{\neq} = 16.3$ kcal/mol) to give IM11, in which the cyclic fructose is generated. The optimized structures of

Scheme 3. Free energy profiles for the isomerization process from the open-chain form of glucose to the open-chain isomer of fructose (step 2) in stage I. Values in kcal/mol are free energies and enthalpies (in the brackets), respectively. [Color figure can be viewed at wileyonlinelibrary.com]

1602 *J. Comput. Chem.* **2019**, *40*, 1599–1608
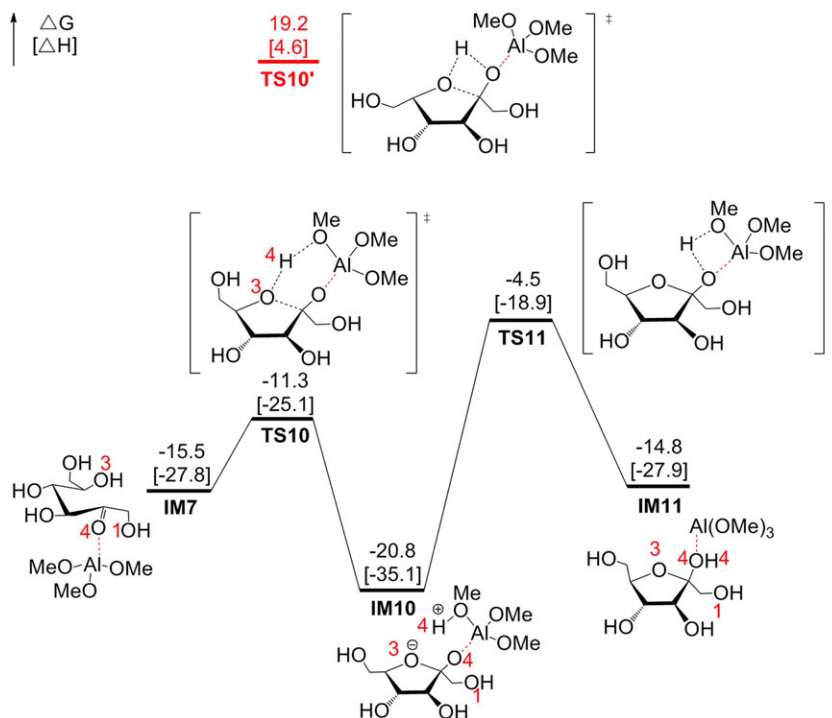
WWW.CHEMISTRYVIEWS.COM ChemistryViews
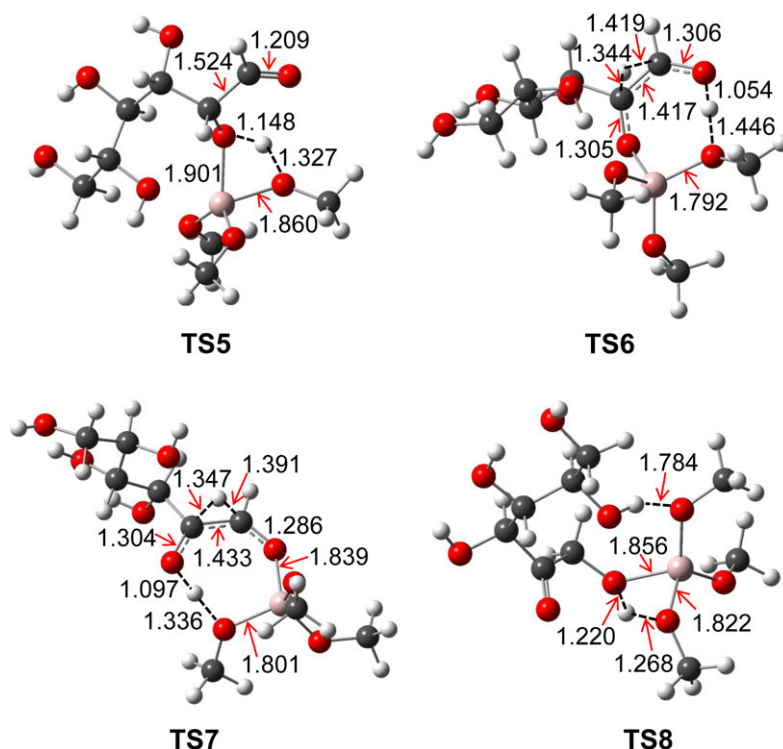
Figure 2. Optimized structures of some important transition states, along with the key bond distances in Å. Other structures are given in Supporting Information Figure S2. Trivial hydrogen atoms are omitted for clarity (color code, C: black, H: white, O: red, Al: pink). [Color figure can be viewed at wileyonlinelibrary.com]

TS10 and TS11 are shown in Figure 3. Similar to the ring-opening process in step 1, the direct ring-closure pathway via TS10' can be easily excluded because of the high barrier of 34.7 kcal/mol. The step from IM7 to IM11 is endothermic by 0.7 kcal/mol, implying the reversible process and IM11 can even be easily converged to the thermodynamically slightly stable IM7. This agrees that only trace amount of fructose could be detected in the experiment. Nonetheless, as expected, the subsequent steps in stage II are highly exothermic, which can

provide enough thermodynamic driving force for moving the reaction forward.

Stage II: Catalytic conversion of fructose 2 to HMF 3

After generating the cyclic fructose as shown in IM11, dehydration reactions will subsequently take place to release three water molecules and lead to the final product HMF 3. On the basis of the energetic and geometric results, we characterize

Scheme 4. Free energy profiles for the ring-closing step (step 3) in stage I. Values in kcal/mol are free energies and enthalpies (in the brackets), respectively. [Color figure can be viewed at wileyonlinelibrary.com]

TS10   **TS11**
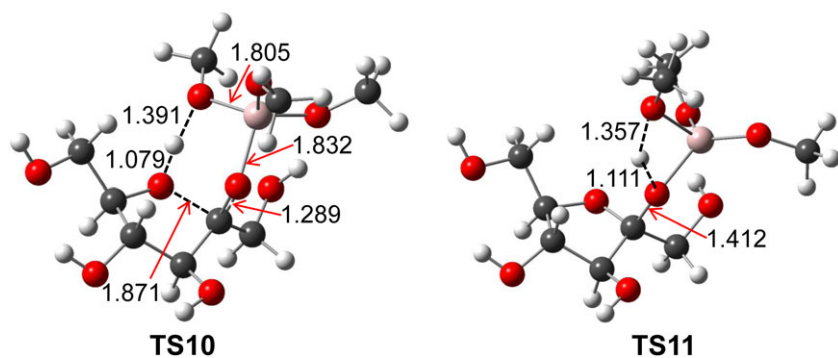
Figure 3. Optimized structures of key stationary points, along with the key bond distances in Å. Other structures are given in Supporting Information Figure S3. Trivial hydrogen atoms are omitted for clarity (color code, C: black, H: white, O: red, Al: pink). [Color figure can be viewed at wileyonlinelibrary.com]

the detailed mechanism of stage II in terms of the following three steps: (1) release the first water molecule via 1,2-elimination to form enolate B (i.e., IM15); (2) release the second water molecule to generate acrolein moiety D (i.e., IM17); and (3) release the third water molecule to produce the final product HMF 3.

Step 1: Release the first H_2O molecule via 1,2-elimination to form enolate B. The energy diagram shown in Scheme 5 describes the detailed reaction mechanism for this step, and the optimized structures of key transition states are displayed in Figure 4.

To release the first H_2O molecule, the catalyst $Al(OMe)_3$ in IM11 needs to slightly adjust its position via TS12 to give the thermodynamically more stable IM12. The H4-atom of the —OH group that bonding to $Al(OMe)_3$ in IM12 can be further transferred to the nearby –OMe ligand via TS13 with a barrier of 11.1 kcal/mol leading to IM13. In TS13, the O—H—O distances are 1.225 and 1.240 Å (Fig. 4), respectively, confirming the

correct hydrogen shift process. Subsequent to the formation of IM13, the reaction needs to overcome the transition state TS14 and TS15 to liberate one water molecule, and the corresponding barriers are 17.9 and 16.8 kcal/mol, respectively. Related to the more stable IM13, the barrier for TS15 is 31.2 kcal/mol, which is slightly higher but still accessible for experimental realization under high temperature (i.e., 120 °C). Note that the direct dehydration from IM12 via TS13' can be easily excluded because of the very high reaction barrier (i.e., 68.2 kcal/mol). The formation of the enolate B (i.e., IM15) intermediate is exothermic by 14.8 kcal/mol, which is the anion form of (2R,E)-2-(hydroxymethyl)-5-(hydroxymethylene)tetrahydrofuran-3,4-diol.
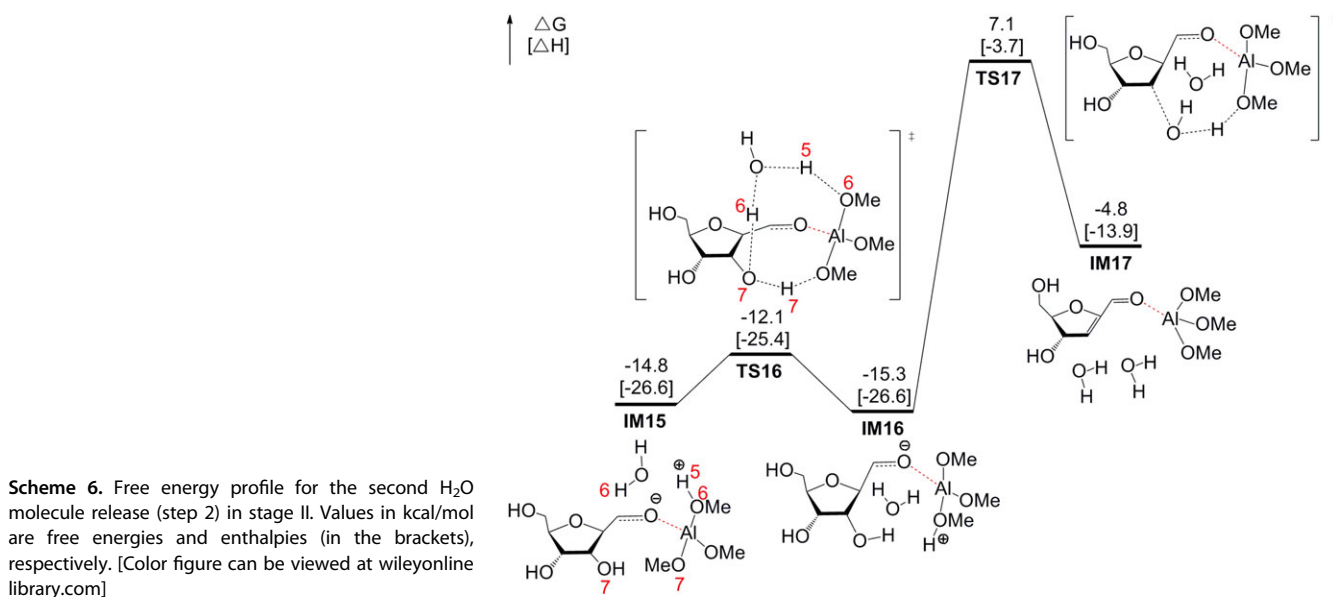
Step 2: Release the second H_2O molecule to generate the acrolein moiety D. After reaching enolate B (i.e., IM15), the released H_2O molecule then adjusts its position by passing a very low barrier of 2.7 kcal/mol (see Scheme 6). In TS16, the activated H5-atom on the —OMe ligand of $Al(OMe)_3$ is transferred to another —OMe ligand with the assistance of long-
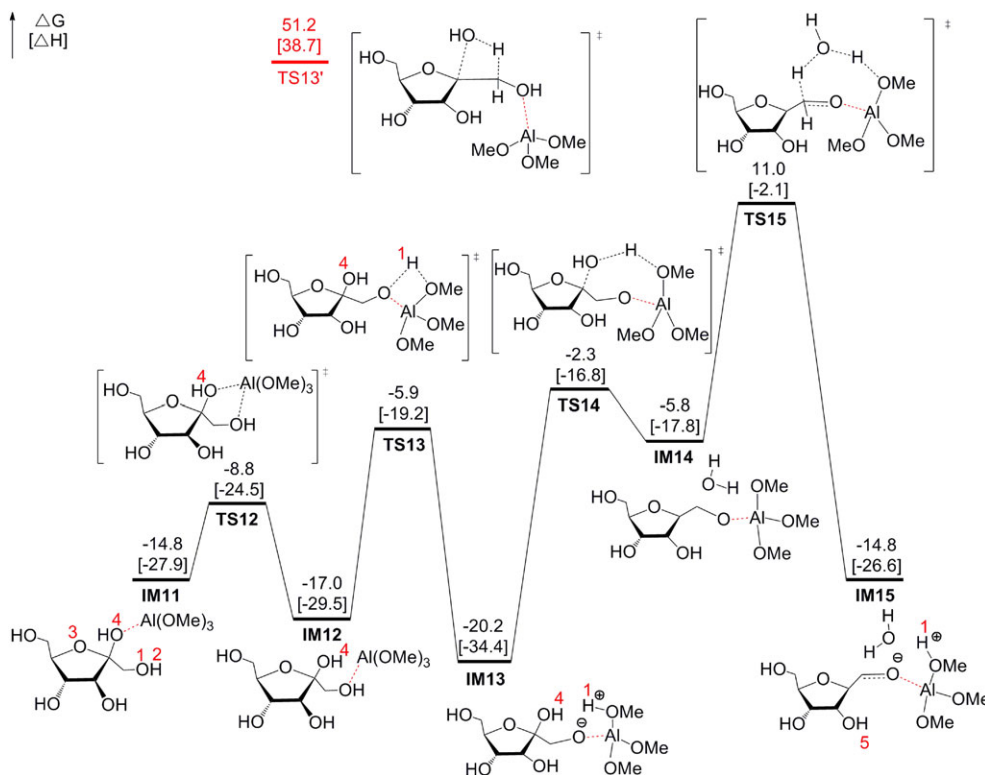
Scheme 5. Free energy profile for the first H_2O molecule release (step 1) in stage II. Values in kcal/mol are free energies and enthalpies (in the brackets), respectively. [Color figure can be viewed at wileyonlinelibrary.com]
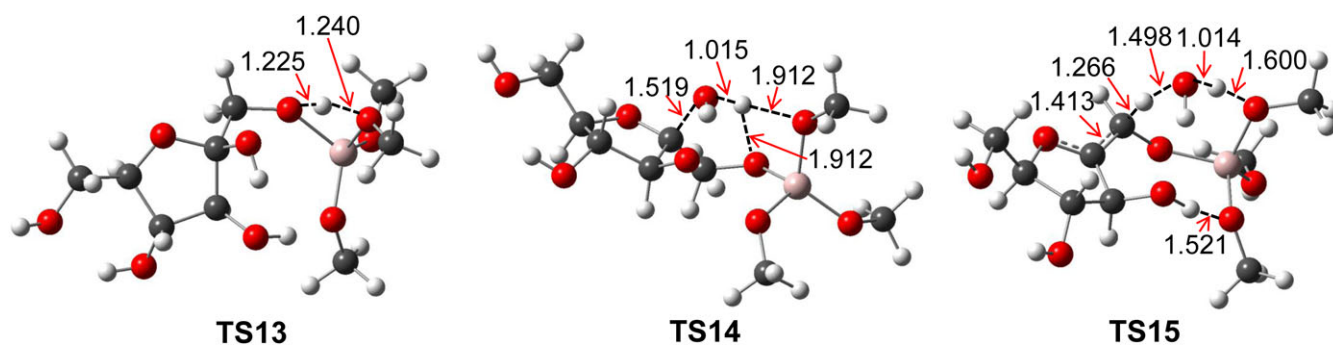
Figure 4. Optimized structures of key stationary points according to Scheme 5, along with the key bond distances in Å. Other structures are given in Supporting Information Figure S4. Trivial hydrogen atoms are omitted for clarity (color code, C: black, H: white, O: red, Al: pink). [Color figure can be viewed at wileyonlinelibrary.com]
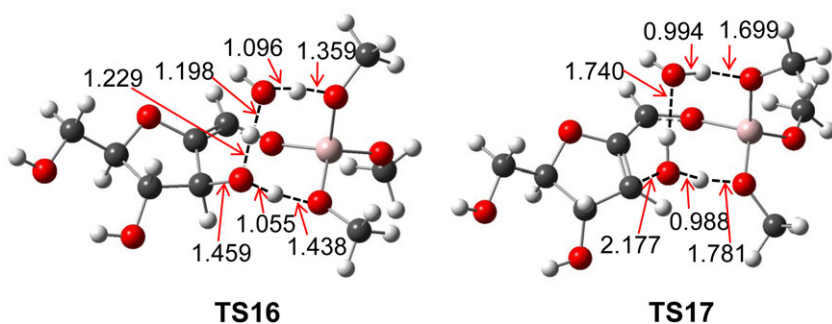

Scheme 6. Free energy profile for the second H_2O molecule release (step 2) in stage II. Values in kcal/mol are free energies and enthalpies (in the brackets), respectively. [Color figure can be viewed at wileyonline library.com]

range hydrogen-bonding interactions, which is confirmed by the changed bond distances (1.359, 1.096, 1.198, 1.229, 1.055, and 1.438 Å, respectively) shown in TS16 (Fig. 5). The generated IM16 is only 0.5 kcal/mol more stable than IM15, suggesting the reversible transformation process. With the assistance of the first released H_2O molecule and the –OMe ligand of $Al(OMe)_3$, the second H_2O molecule could be easily liberated from IM16 via TS17 to generate the acrolein moiety IM17 (i.e., D). The barrier for the second H_2O molecule release is predicted to be 22.4 kcal/mol, which is much less than the first H_2O molecule liberation with a barrier of 31.2 kcal/mol. The optimized TS17 in Figure 5 indicated that the long-range hydrogen-bonding

interactions play significant role in stabilizing the structure, and H_2O acts as the product, reactant, proton shuttle, as well as stabilizer during the transformation process.

Step 3: Release the third water molecule to produce the final product HMF 3. As illustrated by the energetics and geometrics in Scheme 7, the released two H_2O molecules and the catalyst $Al(OMe)_3$ will firstly liberate from IM17 (i.e., D) to give the less stable intermediate IM18. The *in stiu* generated IM18 bonds to $Al(OMe)_3$ facilely giving IM19, which can then be transformed to the more stable IM20 via a low barrier of 8.4 kcal/mol (TS18). Note that the –OMe ligand of $Al(OMe)_3$ is important

Figure 5. Optimized structures of key stationary points according to Scheme 6, along with the key bond distances in Å. Other optimized structures are given in Supporting Information Figure S5. Trivial hydrogen atoms are omitted for clarity (color code, C: black, H: white, O: red, Al: pink). [Color figure can be viewed at wileyonlinelibrary.com]

Wiley Online Library

*J. Comput. Chem.* **2019**, *40*, 1599–1608   **1605**
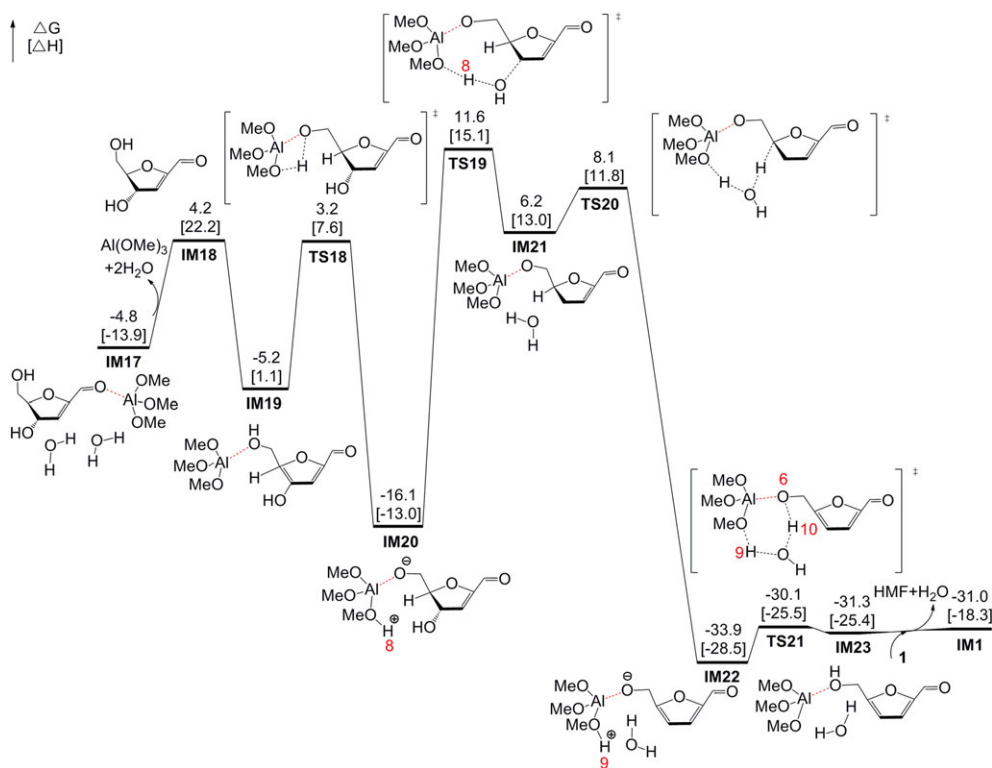
Scheme 7. Free energy profiles for the third H_2O molecule release (step 3) in the stage II. Values in kcal/mol are free energies and enthalpies (in the brackets), respectively. [Color figure can be viewed at wileyonlinelibrary.com]

for abstracting the H-atom in the –OH group, which is illustrated by the optimized geometry of TS18 in Figure 6. On the other hand, we also considered the direct dehydration from IM17 without releasing the two H_2O molecules and the catalyst. However, the very high barriers (see Supporting Information Scheme S2 for details) precluded such reaction pathways.

Subsequent to the formation of IM20, the third water molecule was formed mediated by the metal–ligand bifunctional $Al(OMe)_3$ catalyst. The two barriers for the hydrogen transfer (H8-transfer) and water release process are 27.7 (TS19) and

1.9 kcal/mol (TS20), respectively. In addition, the water molecule assisted hydrogen transfer process was further considered. However, the barrier of TS19-H_2O and TS20-H_2O is slightly unfavorable than TS19 and TS20 (see Supporting Information Scheme S3 for details). The process of IM20 → IM22 is highly exothermic by17.8 kcal/mol. Therefore, the hydrogen shift and water formation process is both kinetically and thermodynamically favorable. With the assistance of the released H_2O molecule, the activated H9-atom on the –OMe ligand of $Al(OMe)_3$ can be further transferred to the O6-atom attached to the Al-
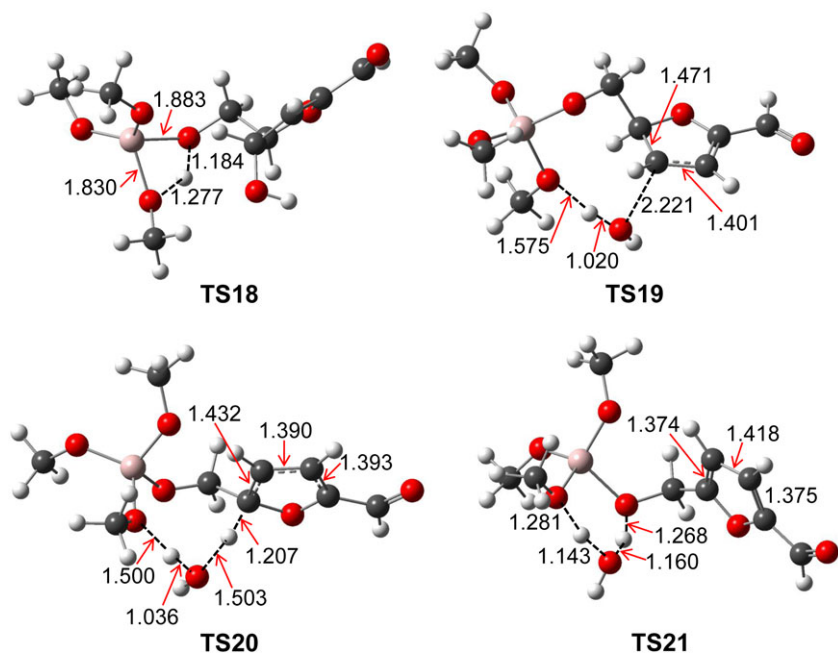
Figure 6. Optimized structures of key stationary points according to Scheme 7, along with the key bond distances in Å. Other structures are given in Supporting Information Figure S6. Trivial hydrogen atoms are omitted for clarity (color code, C: black, H: white, O: red, Al: pink). [Color figure can be viewed at wileyonlinelibrary.com]
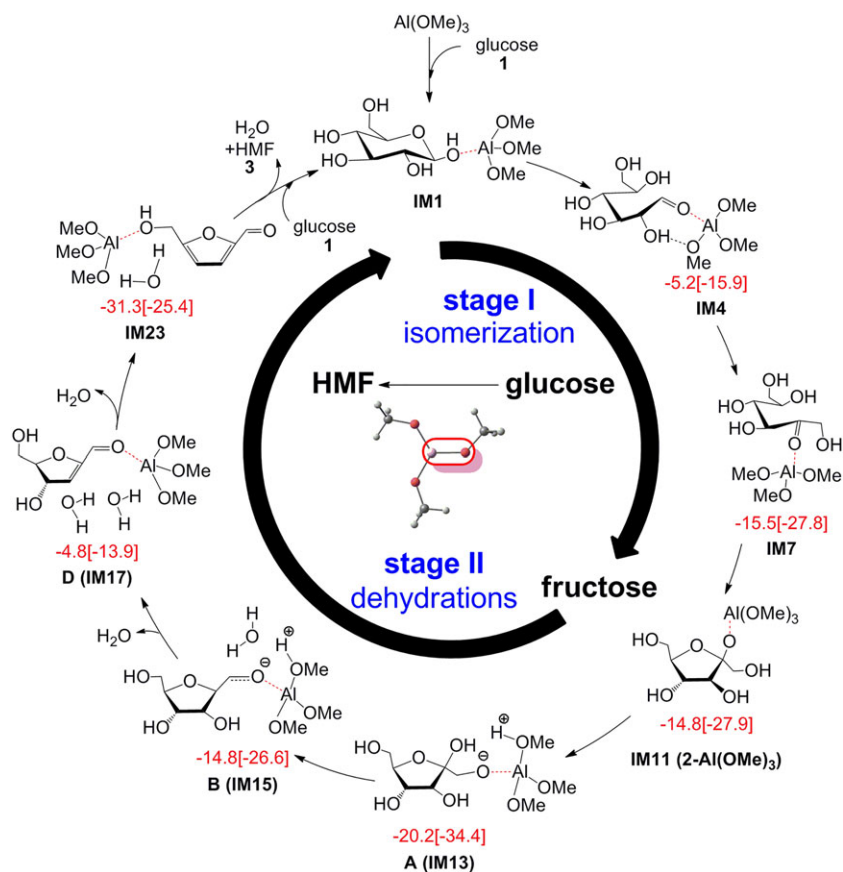
Figure 7. Complete catalytic cycle for the Al(OMe)₃-catalyzed conversation of glucose 1 to HMF 3 via fructose 2. [Color figure can be viewed at wileyonlinelibrary.com]

atom via a long-range hydrogen-bonding interaction TS21 (Fig. 6) to generate the intermediate IM23, in which the final product HMF is produced. Although the liberation of free HMF from IM23 is endothermic, the regenerated catalyst Al(OMe)₃ will react with the initial reactant glucose 1 starting the next catalytic cycle, which can provide enough thermodynamic driving force to reach the final product.

On the basis of the discussions on the Al(OMe)₃-catalyzed target reaction, we assemble the two stages together to give the most favorable catalytic cycle in Figure 7. Each stage is kinetically and thermodynamically feasible. The barrier (TS15) for abstracting the —OH group and forming the first water molecule is the highest ($\Delta G^{\neq}$ = 31.2 kcal/mol), which is demonstrated to be the rate-determining step in the whole catalysis. It is worthy of mentioning that the long-range hydrogen-bond interactions among the catalyst, reactant, and the released water molecules play important role in the whole catalytic process and the released H_2O molecules act as the product, reactant, proton shuttle, and stabilizer during the reaction pathway. In addition, the metal–ligand bifunctional effects in the catalyst Al(OMe)₃ play crucial role in stabilizing the intermediates and transition states during the whole catalytic cycle.

Conclusion

In conclusion, DFT calculations were performed to understand the detailed reaction mechanism of Al(OMe)₃-catalyzed conversation of glucose to HMF. Our study reveals that the reaction

takes place via two stages, including the catalytic isomerization of glucose to fructose (stage I) and the catalytic transformation of fructose to HMF (stage II). There are three steps involved in stage I, which include (1) ring-opening of cyclic pyranose 1 to its open-chain isomer; (2) isomerization from the open-chain form of glucose to the open-chain isomer of fructose via long-range intermolecular hydrogen-bonding interactions; and (3): ring-closure generating cyclic fructose 2. The highest barrier in stage I is predicted to be 23.9 kcal/mol (i.e., IM2 → TS6), which is low enough for experimental realization under mild conditions. There are also three steps in stage II, which includes three successive dehydrations that begins with a 1,2-elimination to form enolate B, continues with the formation of acrolein moiety D, and ends with the formation of the furan ring HMF 3. Each step is kinetically and thermodynamically favorable feasible. The highest barrier in stage II is predicated to be 31.2 kcal/mol (i.e., IM13 → TS15), which is somewhat higher but still experimentally accessible under high temperature (i.e., 120 °C). Stage II is highly exothermic by 31.3 kcal/mol, which can afford enough thermodynamic driving force to reach the final product and release the Al(OMe)₃ catalyst for the next catalytic cycle.

Our mechanistic study affords further insights on the origin of high reactivity of the catalyst. On the one hand, the metal–ligand bifunctional effects in the Al(OMe)₃ catalyst play critical role in stabilizing the intermediates and transition states during the reaction pathway. The alkoxy-oxygen is the Lewis base and can be protonated by alcohols or activated C—H bonds. On the other hand, the released water molecules in stage II act as

Wiley Online Library

J. Comput. Chem. **2019**, *40*, 1599–1608   **1607**

product, reactant, proton shuttle, as well as stabilizer in the conversion of fructose to HMF. Finally, the long-range hydrogen-bonding interactions among the catalyst, reactant, and the released water molecules are helpful to improve the kinetics and thermodynamics for the whole catalysis.

Acknowledgment

Keywords: DFT calculations · reaction mechanism · glucose · HMF · aluminum alkoxy catalyst

[1] D. M. Alonso, J. Q. Bond, J. A. Dumesic, *Green Chem.* **2010**, *12*, 1493.
[2] M. Stöcker, *Angew. Chem. Int. Ed.* **2008**, *47*, 9200.
[3] A. Corma, S. Iborra, A. Velty, *Chem. Rev.* **2007**, *107*, 2411.
[4] A. Mukherjee, M. J. Dumont, V. Raghavan, *Biomass Bioenergy* **2015**, *72*, 143.
[5] D. J. Liu, E. Y. X. Chen, *ACS Catal.* **2014**, *4*, 1302.
[6] J. L. Song, H. L. Fan, J. Ma, B. X. Han, *Green Chem.* **2013**, *15*, 2619.
[7] Z. R. Zhang, J. L. Song, B. X. Han, *Chem. Rev.* **2017**, *117*, 6834.
[8] Z. H. Mou, S. Feng, E. Y. X. Chen, *Polym. Chem.* **2016**, *7*, 1593.
[9] P. Zhou, Z. H. Zhang, *Catal. Sci. Technol.* **2016**, *6*, 3694.
[10] S. Leng, X. D. Wang, Q. X. Cai, F. Y. Ma, Y. E. Liu, J. G. Wang, *Bioresour. Technol.* **2013**, *149*, 341.
[11] L. P. Zhou, Z. Liu, M. T. Shi, S. S. Du, Y. L. Su, X. M. Yang, J. Xu, *Carbohydr. Polym.* **2013**, *98*, 146.
[12] D. J. Liu, Y. T. Zhang, E. Y. X. Chen, *Green Chem.* **2012**, *14*, 2738.
[13] L. T. Mika, E. Csefalvay, A. Nemeth, *Chem. Rev.* **2018**, *118*, 505.
[14] B. M. Upton, A. M. Kasko, *Chem. Rev.* **2016**, *116*, 2275.
[15] C. Sievers, I. Musin, T. Marzialetti, M. B. Valenzuela Olarte, P. K. Agrawal, C. W. Jones, *Chemsuschem* **2009**, *2*, 665.
[16] S. Lima, P. Neves, M. M. Antunes, M. Pillinger, N. Ignatyev, A. A. Valente, *Appl. Catal. A-Gen.* **2009**, *363*, 93.
[17] D. Liu, E. Y. X. Chen, *Appl. Catal. A-Gen.* **2012**, *435*, 78.
[18] T. A. Werpy, G. Petersen, T. *Value Added, Top Value Added Chemicals From Biomass* **2004**, *1*, p1–66.
[19] Y. Román-Leshkov, C. J. Barrett, Z. Y. Liu, J. A. Dumesic, *Nature* **2007**, *447*, 982.
[20] Q.-N. Xia, Q. Cuan, X.-H. Liu, X.-Q. Gong, G.-Z. Lu, Y.-Q. Wang, *Angew. Chem. Int. Ed.* **2014**, *53*, 9755.
[21] J. Artz, R. Palkovits, *Chemsuschem* **2015**, *8*, 3832.
[22] D. Sun, S. Sato, W. Ueda, A. Primo, H. Garcia, A. Corma, *Green Chem.* **2016**, *18*, 2579.
[23] X. Qi, M. Watanabe, T. M. Aida, J. R. L. Smith, *Green Chem.* **2009**, *11*, 1327.
[24] T. S. Hansen, J. M. Woodley, A. Riisager, *Carbohydr. Res.* **2009**, *344*, 2568.
[25] N. Yoshio, M. Shunichi, *Bull. Chem. Soc. Jpn.* **1980**, *53*, 3705.
[26] Y. Yuan, S. Q. Yao, S. X. Nie, S. F. Wang, *Bioresources* **2016**, *11*, 2381.
[27] A. S. Amarasekara, A. Razzaq, *Carbohydr. Res.* **2014**, *386*, 86.
[28] D. J. Liu, E. Y. X. Chen, *Chemsuschem* **2013**, *6*, 2236.
[29] S. Kei-ichi, I. Yoshihisa, I. Hitoshi, *Bull. Chem. Soc. Jpn.* **2001**, *74*, 1145.
[30] H. Ishida, K.-i. Seri, *J. Mol. Catal. A-Chem.* **1996**, *112*, L163.
[31] S. Kei-ichi, I. Yoshihisa, I. Hitoshi, *Chem. Lett.* **2000**, *29*, 22.
[32] H. Zhao, J. E. Holladay, H. Brown, Z. C. Zhang, *Science* **2007**, *316*, 1597.
[33] G. Yong, Y. Zhang, J. Y. Ying, *Angew. Chem. Int. Ed.* **2008**, *47*, 9345.
[34] E. A. Pidko, V. Degirmenci, R. A. van Santen, E. J. M. Hensen, *Angew. Chem. Int. Ed.* **2010**, *49*, 2530.
[35] D. J. Liu, E. Y. X. Chen, *Biomass Bioenergy* **2013**, *48*, 181.
[36] J. H. He, Y. T. Zhang, E. Y. X. Chen, *Chemsuschem* **2013**, *6*, 61.
[37] L. Q. Wu, J. L. Song, B. B. Zhang, B. W. Zhou, H. C. Zhou, H. L. Fan, Y. Y. Yang, B. X. Han, *Green Chem.* **2014**, *16*, 3935.
[38] E. F. Dunn, D. J. Liu, E. Y. X. Chen, *Appl. Catal. A-Gen.* **2013**, *460*, 1.
[39] J. L. Song, B. B. Zhang, J. H. Shi, H. L. Fan, J. Ma, Y. Y. Yang, B. X. Han, *Rsc. Adv.* **2013**, *3*, 20085.
[40] F. D'Anna, S. Marullo, P. Vitale, C. Rizzo, R. Lo Meo, R. Noto, *Appl. Catal. A-Gen.* **2014**, *482*, 287.
[41] D. J. Liu, E. Y. X. Chen, *Green Chem.* **2014**, *16*, 964.
[42] S. Hu, Z. Zhang, J. Song, Y. Zhou, B. Han, *Green Chem.* **2009**, *11*, 1746.
[43] M. Chidambaram, A. T. Bell, *Green Chem.* **2010**, *12*, 1253.
[44] A. Teimouri, M. Mazaheri, A. N. Chermahini, H. Salavati, F. Momenbeik, M. Fazel-Najafabadi, *Taiwan. Inst. Chem. E* **2015**, *49*, 40.
[45] H. Matsumiya, T. Hara, *Biomass Bioenergy* **2015**, *72*, 227.
[46] H. T. Han, H. Y. Zhao, Y. Liu, Z. F. Li, J. Y. Song, W. Y. Chu, Z. Z. Sun, *Rsc. Adv.* **2017**, *7*, 3790.
[47] Y. Zhang, H. Du, X. Qian, E. Y. X. Chen, *Energy Fuels* **2010**, *24*, 2410.
[48] D. Saang'onyo, S. Parkin, F. T. Ladipo, *Polyhedron* **2018**, *149*, 153.
[49] M. J. Frisch, et al., Gaussian 09, Revision A.01, Gaussian, Inc., Wallingford, CT, **2009**.
[50] C. Lee, W. Yang, R. G. Parr, *Phys. Rev. B* **1988**, *37*, 785.
[51] A. D. Becke, *J. Chem. Phys.* **1993**, *98*, 5648.
[52] Y. Zhao, D. G. Truhlar, *Theor. Chem. Acc.* **2008**, *120*, 215.
[53] E. Cancès, B. Mennucci, J. Tomasi, *J. Chem. Phys.* **1997**, *107*, 3032.
[54] B. Mennucci, J. Tomasi, *J. Chem. Phys.* **1997**, *106*, 5151.
[55] B. Mennucci, E. Cancès, J. Tomasi, *J. Phys. Chem. B* **1997**, *101*, 10506.
[56] J. Tomasi, B. Mennucci, E. Cancès, *J. Mol. Struct.* **1999**, *464*, 211.
[57] A. K. Rappe, C. J. Casewit, K. S. Colwell, W. A. Goddard, W. M. Skiff, *J. Am. Chem. Soc.* **1992**, *114*, 10,024.
[58] A. E. Stearn, H. Eyring, *J. Chem. Phys.* **1937**, *5*, 113.